IOP Conf. Series: Materials Science and Engineering **192** (2017) 012003 doi:10.1088/1757-899X/192/1/012003

On the theory of unsteady-state crystallization with a mushy layer

D V Alexandrov, I V Alexandrova and A A Ivanov

Department of Theoretical and Mathematical Physics, Laboratory of Multi-Scale Mathematical Modeling, Ural Federal University, Ekaterinburg, 620000, Russian Federation

E-mail: dmitri.alexandrov@urfu.ru

Abstract. The self-similar and unsteady-state crystallization processes of binary melts with a mushy layer are considered. Two analytical methods of solution of the mushy layer nonlinear model with the moving phase transition boundaries are detailed. The obtained analytical solutions are in good agreement with experimental data.

1. Introduction

It is well-known that crystallization processes play a key role in materials science and determine different properties of solidified liquids and melts [1–3]. A standard description of crystallization by means of the classical Stefan thermodiffusion model with a planar solid-liquid interface works well far from always. This is explained by the fact that, in the certain circumstances, a supercooled two-phase (mushy) layer arises ahead of a moving crystallization front [4–6]. As a result of this phenomenon, after a lapse of time, a crystallization domain becomes divided into three regions: solid phase, mushy layer and liquid phase. In other words, a mushy layer represents a region of morphological instability [7–10]. Due to the effect of constitutional supercooling, different elements of the solid phase in the form of nuclei or dendrite-like structures become capable to evolve in the mushy layer. Their evolution accompanied by the released latent heat of solidification will compensate the constitutional supercooling and the mushy layer as a whole will evolve in a non-equilibrium manner [11–13]. If the latent heat of crystallization completely compensates the constitutional supercooling, the mushy layer is termed as quasiequilibrium. A theoretical description of this crystallization scenario was developed in [14–16]. A mathematical model describing these solidification conditions represents a set of non-linear differential equations supplemented by the corresponding boundary conditions imposed at the moving interfaces. In the case of steady-state solidification regime, this model admits an exact solution [17–19] in the presence and absence of different non-linear effects such as a weak convection, thermodiffusion and temperature-dependent diffusivity. A time-dependent solidification scenario frequently met in practice is very important too. Two original methods of analytical solutions of the non-linear transient mushy layer equations were developed in a series of papers [20–24]. The present study is concerned with generalization of these methods for the description of unsteady-state crystallization regimes.

The outline of this paper is as follows: Section 2 is devoted to a theoretical description of self-similar solidification process with a planar front and as well as with a mushy layer; an analytical

approach for the transient solidification conditions is described in Section 3; a summary of results and conclusions are presented in Section 4.

2. Self-similar crystallization scenario

Let us consider a unidirectional crystallization process of a binary mixture from a cooled wall shown in Figure 1 (z being the solidification direction). The semi-infinite domain $z > 0$ filled with the liquid phase is initially maintained at the constant temperature T_∞ and has the uniform impurity concentration $C = c_0$. Let us also neglect the diffusion transport in the solid phase as well as the gravitational force. The temperature of the cooled wall $z = 0$ equals $T = T_B$, which is lower than the liquidus temperature.

2.1. Self-similar regime with a planar front

The temperature (T) and concentration (C) distributions in the solid ($0 < z < h(t)$) and liquid ($z > h(t)$) phases are governed by the following transfer equations

$$\rho_s C_{ps} \frac{\partial T}{\partial t} = k_s \frac{\partial^2 T}{\partial z^2},\ 0 < z < h(t), \tag{1}$$

$$\rho_l C_{pl} \frac{\partial T}{\partial t} = k_l \frac{\partial^2 T}{\partial z^2},\ \frac{\partial C}{\partial t} = D \frac{\partial^2 C}{\partial z^2},\ z > h(t), \tag{2}$$

where ρ_s and ρ_l are the densities of the solid and liquid phases, C_{ps} and C_{pl} are the specific heats in these phases, D is the diffusion coefficient, and $h(t)$ is the solid-liquid interface coordinate, which moves into the liquid region and depends on time t.

The wall temperature is fixed

$$T = T_B,\ z = 0, \tag{3}$$

and the far-field boundary conditions take the form

$$T \to T_\infty,\ C \to c_0,\ z \to \infty. \tag{4}$$

At the moving phase transition interface, we have the following liquidus and balance conditions

$$T = -mC,\ z = h(t), \tag{5}$$

$$\rho_s L \frac{dh}{dt} = k_s \left(\frac{\partial T}{\partial z}\right)_{z=h^-} - k_l \left(\frac{\partial T}{\partial z}\right)_{z=h^+},\ z = h(t), \tag{6}$$

$$C \frac{dh}{dt} + D \left(\frac{\partial C}{\partial z}\right)_{z=h^+} = 0,\ z = h(t). \tag{7}$$

Here m is the liquidus slope, L is the latent heat of solidification, and subscripts h^- and h^+ designate the solid and liquid sides of the moving front $h(t)$.

The moving-boundary problem (1)-(7) can be solved by means of introducing the self-similar variable η and the parabolic growth rate constant λ

$$\eta = \frac{z}{\sqrt{4Dt + s}},\ \lambda = \frac{h(t)}{\sqrt{4Dt + s}}, \tag{8}$$

where $s = h^2(0)/\lambda^2$, and λ represents the self-similar solid-liquid interface.

The self-similar solutions of equations (1)-(7) can be written out as [20, 25]

$$T(\eta) = T_B + \frac{(T_h - T_B)\mathrm{erf}(\varepsilon_s \eta)}{\mathrm{erf}(\varepsilon_s \lambda)},\ \eta < \lambda, \tag{9}$$

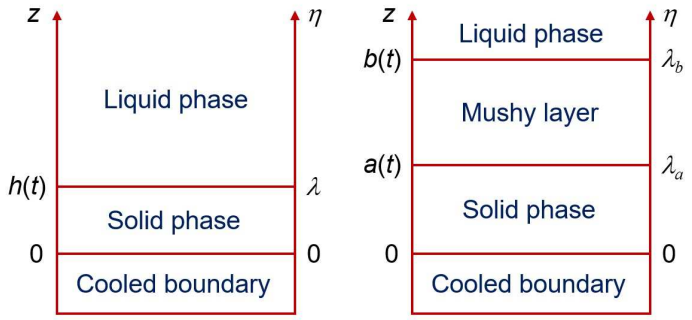

Figure 1. A scheme of solidification process with a planar front and mushy layer.

$$T(\eta) = T_\infty + \frac{(T_h - T_\infty)\mathrm{erfc}(\varepsilon_l \eta)}{\mathrm{erfc}(\varepsilon_l \lambda)},\ \eta > \lambda, \tag{10}$$

$$C(\eta) = c_0 + \frac{(C_h - c_0)\mathrm{erfc}(\eta)}{\mathrm{erfc}(\lambda)},\ \eta > \lambda, \tag{11}$$

where T_h and C_h designate the temperature and concentration at the front $\eta = \lambda$, $\varepsilon_s = \sqrt{DC_{ps}\rho_s/k_s}$, and $\varepsilon_l = \sqrt{DC_{pl}\rho_l/k_l}$.

Three unknown parameters T_h, C_h and λ can be found from the boundary conditions (5)-(7) in the form

$$T_h = -mC_h,\ C_h - c_0 = C_{fi}(\lambda) \equiv \frac{c_0 F(\lambda)}{1 - F(\lambda)}, \tag{12}$$

$$mC_{fi}(\lambda)\left[\frac{\beta}{F(\varepsilon_l\lambda)} + \frac{1}{G(\varepsilon_s\lambda)}\right] = \frac{T_1}{G(\varepsilon_s\lambda)} - \frac{\beta T_0}{F(\varepsilon_l\lambda)} - \frac{L}{C_{ps}}. \tag{13}$$

Here we used the following designations

$$\beta = \frac{\rho_l C_{pl}}{\rho_s C_{ps}},\ F(x) = \sqrt{\pi}x\exp(x^2)\mathrm{erfc}(x),\ G(x) = \sqrt{\pi}x\exp(x^2)\mathrm{erf}(x).$$

The self-similar front position is determined by equation (13). Note that a behavior of λ as well as the temperature differences $T_1 = -mc_0 - T_B$ and $T_0 = T_\infty + mc_0$ has been demonstrated in [25].

The constitutional supercooling appears ahead of the planar solid-liquid interface when the concentration gradient becomes greater than the temperature one at $z = h^+$, that is

$$\frac{\partial T}{\partial z} < -m\frac{\partial C}{\partial z},\ z = h^+. \tag{14}$$

Substitution of analytical solutions (10) and (11) into inequality (14) gives

$$C_{fi}(\lambda) > C_i(\lambda) \equiv \frac{(T_0/m)\,\varepsilon_l^2 F(\lambda)}{F(\varepsilon_l\lambda) - \varepsilon_l^2 F(\lambda)}. \tag{15}$$

If this inequality holds true, the constitutional supercooling exists ahead of the self-similar solidification front $\eta = \lambda$ and, as a consequence, we must use a mushy layer model instead of the frontal model above.

2.2. Self-similar regime with a mushy layer

In the case of a mushy layer solidification scenario (Figure 1), the heat and mass transfer process in this layer, $a(t) < z < b(t)$, depends on the solid fraction φ and is described by the following transfer equations

$$(\rho C_p)_m \frac{\partial T}{\partial t} = \frac{\partial}{\partial z}\left(k_m \frac{\partial T}{\partial z}\right) + \rho_s L \frac{\partial \varphi}{\partial t},\ T = -mC,\ a(t) < z < b(t), \tag{16}$$

$$\chi \frac{\partial C}{\partial t} = \frac{\partial}{\partial z}\left(D\chi \frac{\partial C}{\partial z}\right) + C\frac{\partial \varphi}{\partial t},\ \chi = 1-\varphi,\ a(t) < z < b(t), \tag{17}$$

where χ represents the liquid fraction of a mushy layer and the thermal properties of a mush are assumed to be volume-fraction weighted averages of the properties of the solid and liquid phases [26], i.e.

$$(\rho C_p)_m = \chi \rho_l C_{pl} + (1-\chi)\rho_s C_{ps},\ k_m = \chi k_l + (1-\chi)k_s.$$

The heat and mass balance boundary conditions imposed at the solid - mushy layer ($z = a(t)$) and mushy layer - liquid ($z = b(t)$) interfaces can be written out as follows

$$\rho_s L \chi_a \frac{da}{dt} = k_s \left(\frac{\partial T}{\partial z}\right)_{z=a^-} - k_m \left(\frac{\partial T}{\partial z}\right)_{z=a^+},\ C_a \chi_a \frac{da}{dt} = -D\chi_a \left(\frac{\partial C}{\partial z}\right)_{z=a^+},$$

$$\rho_s L\,(1-\chi_b)\,\frac{db}{dt} = k_m \left(\frac{\partial T}{\partial z}\right)_{z=b^-} - k_l \left(\frac{\partial T}{\partial z}\right)_{z=b^+}, \tag{18}$$

$$C_b\,(1-\chi_b)\,\frac{db}{dt} = D\chi_b \left(\frac{\partial C}{\partial z}\right)_{z=b^-} - D \left(\frac{\partial C}{\partial z}\right)_{z=b^+},$$

where subscripts a^- and a^+ designate the solid and mushy layer sides of the phase transition boundary $z = a(t)$, whereas b^- and b^+ designate the mushy layer and liquid sides of the second boundary $z = b(t)$.

A condition of marginal equilibrium reads as

$$\frac{\partial T}{\partial z} = -m\frac{\partial C}{\partial z},\ z = b^+. \tag{19}$$

The last condition demonstrates that none of the liquid layer, $z > b(t)$, is supercooled.

Let us introduce the following self-similar variables by analogy with (8)

$$\lambda_a = \frac{a(t)}{\sqrt{4Dt+s}},\ \lambda_b = \frac{b(t)}{\sqrt{4Dt+s}}, \tag{20}$$

where the parabolic growth rate constants λ_a and λ_b determine the self-similar coordinates of a mushy layer.

A nonlinear set of equations and boundary conditions (16)-(19) can be rewritten in the self-similar variables (8) and (20) as

$$-2\eta(1-\varphi)\frac{dC}{d\eta} = -\frac{d\varphi}{d\eta}\frac{dC}{d\eta} + (1-\varphi)\frac{d^2C}{d\eta^2} - 2\eta C\frac{d\varphi}{d\eta},\ \alpha = \frac{mC_{ps}}{L},\ \lambda_a < \eta < \lambda_b, \tag{21}$$

$$-2\alpha\varepsilon_s^2\left[\beta + (1-\beta)\varphi\right]\eta\frac{dC}{d\eta} = \left[\Lambda + \Lambda_1\varphi\right]\alpha\frac{d^2C}{d\eta^2} + \alpha\Lambda_1\frac{d\varphi}{d\eta}\frac{dC}{d\eta} + 2\varepsilon_s^2\eta\frac{d\varphi}{d\eta},\ \lambda_a < \eta < \lambda_b, \tag{22}$$

$$C = c_0 + C_i(\lambda_b),\ \eta = \lambda_b;\ \Lambda = \frac{k_l}{k_s},\ \Lambda_1 = 1 - \Lambda, \tag{23}$$

$$\left[\frac{\varepsilon_s^2 \chi_b}{\alpha} + \frac{k_m(\chi_b)}{k_s} C_b - \frac{C_i(\lambda_b)}{F(\lambda_b)}\right](1 - \chi_b) = 0,\ \eta = \lambda_b, \tag{24}$$

$$\frac{dC}{d\eta} = -2\lambda_b \left[\frac{k_l}{k_m(\chi_b)} \frac{C_i(\lambda_b)}{F(\lambda_b)} + \frac{\varepsilon_s^2}{\alpha} \frac{k_s}{k_m(\lambda_b)}(1 - \chi_b)\right],\ \eta = \lambda_b, \tag{25}$$

$$\left[2\lambda_a \frac{\varepsilon_s^2 \chi_a}{\alpha} - \frac{k_m(\chi_a)}{k_s} \frac{dC}{d\eta}\right] G(\varepsilon_s \lambda_a) + 2\lambda_a \varepsilon_s^2 \left[C + \frac{T_B}{m}\right] = 0,\ \eta = \lambda_a, \tag{26}$$

$$\left[\frac{dC}{d\eta} + 2\lambda_a C\right] \chi_a = 0,\ \eta = \lambda_a. \tag{27}$$

The boundary condition (24) implies that either $\chi_b = 1$ or

$$\chi_b \equiv \chi_i = \frac{c_0 \left[C_i(\lambda_b)/C_{fi}(\lambda_b) - 1\right]}{\varepsilon_s^2/\alpha + C_b \left(k_l/k_s - 1\right)}. \tag{28}$$

This makes possible to choose the boundary condition in the form $\chi_b = \chi_i$ if $0 \leq \chi_i < 1$ and $\chi_b = 1$ otherwise [25]. The boundary condition (26) must be considered in the same manner.

Let us seek for the solution of the aforementioned problem in the form of series in η, i.e.

$$\begin{aligned} \varphi(\eta) &= \varphi_0 + \eta\varphi_1 + \eta^2\varphi_2 + \eta^3\varphi_3 ..., \\ C(\eta) &= C_0 + \eta C_1 + \eta^2 C_2 + \eta^3 C_3 + ... \end{aligned} \tag{29}$$

Now substituting expansions (29) into equations (21) and (22), we arrive at two equations in the zero-order approximation in η

$$\varphi_1 C_1 = 2(1 - \varphi_0) C_2,\ 2C_2 \left[\Lambda + (1 - \Lambda)\varphi_0\right] + (1 - \Lambda)\varphi_1 C_1 = 0.$$

These equations show that the solution is trivial, that is $\varphi_1 = 0$ and $C_2 = 0$.

The first-order approximation leads to equations for φ_2 and C_3. Their solution reads as follows

$$\begin{aligned} \varphi_2 &= (1 - \varphi_0)\left[\Lambda + (1 - \Lambda)\varphi_0 - \varepsilon_s^2 \left(\beta + (1 - \beta)\varphi_0\right)\right], \\ C_3 &= L_0(\lambda_b) C_1,\ L_0(\lambda_b) = -\frac{(1 - \Lambda)(1 - \varphi_0) + \varepsilon_s^2 \left[\beta + (1 - \beta)\varphi_0\right]}{3}. \end{aligned} \tag{30}$$

Substitution of solutions (30) into the boundary condition $\varphi(\lambda_b) = \varphi_b = \varphi_0 + \lambda_b^2 \varphi_2$ leads to a quadratic equation for $\varphi_0(\lambda_b)$. Its solution reads

$$\varphi_0(\lambda_b) = \varphi_0^{\pm} = \frac{\pm\sqrt{b_1^2 - 4a_1 c_1} - b_1}{2a_1}, \tag{31}$$

$$a_1(\lambda_b) = \lambda_b^2 \left[1 - \Lambda - \varepsilon_s^2(1 - \beta)\right],\ b_1(\lambda_b) = \left[2\Lambda\lambda_b^2 - \lambda_b^2 - 1 + \varepsilon_s^2 \lambda_b^2 (1 - 2\beta)\right],$$

$$c_1(\lambda_b) = \varphi_b(\lambda_b) - \lambda_b^2 \left(\Lambda - \varepsilon_s^2 \beta\right),\ \varphi_b(\lambda_b) = 1 - \chi_b(\lambda_b).$$

The boundary condition (23) implies that

$$C_0(\lambda_b) = c_0 + C_i(\lambda_b) - \lambda_b C_1 \left[1 + \lambda_b^2 L_0(\lambda_b)\right]. \tag{32}$$

Let us consider the case when $\chi_a \neq 0$. Then we have from condition (27)

$$C_1 = -\frac{2\lambda_a \left[c_0 + C_i(\lambda_b)\right]}{1 + 2\lambda_a^2 - 2\lambda_a\lambda_b + L_0(\lambda_b)\left[3\lambda_a^2 + 2\lambda_a^4 - 2\lambda_a\lambda_b^3\right]}. \tag{33}$$

The boundary condition (25) leads to

$$C_1(\lambda_b) = H_1(\lambda_b),\ H_1(\lambda_b) = -\frac{H(\lambda_b)}{k_m(\lambda_b)\left[1 + 3\lambda_b^2 L_0(\lambda_b)\right]}, \tag{34}$$

$$H(\lambda_b) = 2\lambda_b\left[k_l\frac{C_i(\lambda_b)}{F(\lambda_b)} + \frac{\varepsilon_s^2 k_s}{\alpha}(1-\chi_b)\right].$$

Now the boundary condition (26) gives

$$\left[2\lambda_a\frac{\varepsilon_s^2\chi_a}{\alpha} - \frac{k_m(\chi_a)}{k_s}\left(C_1 + 3\lambda_a^2 C_3\right)\right]G(\varepsilon_s\lambda_a) + 2\lambda_a\varepsilon_s^2\left[C_0 + \lambda_a C_1 + \lambda_a^3 C_3 + \frac{T_B}{m}\right] = 0. \tag{35}$$

Equations (33)-(35) enable us to find λ_a and λ_b.

When $\lambda_a \ll \lambda_b$, one can obtain an explicit solution. In this case, we get from expressions (33) and (34)

$$\lambda_a(\lambda_b) = \frac{\pm\sqrt{r_2^2 - 4r_1H_1} - r_2}{2r_1}, \tag{36}$$

$$r_1(\lambda_b) = H_1(\lambda_b)\left(2 + 3L_0(\lambda_b)\right),\ r_2(\lambda_b) = 2\left[c_0 + C_i(\lambda_b)\right] - 2H_1(\lambda_b)\lambda_b\left(1 + \lambda_b^2 L_0(\lambda_b)\right).$$

Note that our numerical solutions show that equation (36) is valid in the case of its positive root. In this case, equation (35) determines the growth constant λ_b.

Now let us consider the case $\varphi_a = 1$ ($\chi_a = 0$). The coefficints φ_0, φ_2, C_0, C_1 and C_3 can be found as before by means of expressions (30)-(32) and (34), while λ_a is determined by equation $\varphi_0(\lambda_b) + \lambda_a^2\varphi_2(\lambda_b) = 1$. Its solution gives

$$\lambda_a(\lambda_b) = \sqrt{\frac{1 - \varphi_0(\lambda_b)}{\varphi_2(\lambda_b)}}. \tag{37}$$

Note that the analytical solutions of self-similar solidification scenario are described by expressions (24) and (29)-(37).

The obtained analytical solution is demonstrated in Figure 2. A self-similar mushy layer appears a result of constitutional supercooling at a critical point $T_1 > 1.776^{\circ}$C and $\lambda > 0.154$. The method of approximate analytical solutions under consideration is in good agreement with experiments [27]. More detailed analysis of a behavior of analytical solutions in the vicinity of a critical point can be found in [20, 25].

An important point is that we can construct an explicit analytical solution in the limiting case $\varphi \to 1$. In this case, equations (21), (24), (26) and (27) will be satisfied automatically, and equation (22) leads to

$$\frac{d^2C}{d\eta^2} = -2\varepsilon_s^2\eta\frac{dC}{d\eta}.$$

Its integration gives

$$C(\eta) = A\int_{\lambda_b}^{\eta}\exp\left(-\varepsilon_s^2 z_1^2\right)dz_1 + B, \tag{38}$$

where constants A and B are determined from the boundary conditions (23) and (25) so that

$$A = -2\lambda_b\exp\left(\varepsilon_s^2\lambda_b\right)\left[\frac{k_l}{k_s}\frac{C_i(\lambda_b)}{F(\lambda_b)} + \frac{\varepsilon_s^2}{\alpha}\right],\ B = c_0 + C_i(\lambda_b).$$

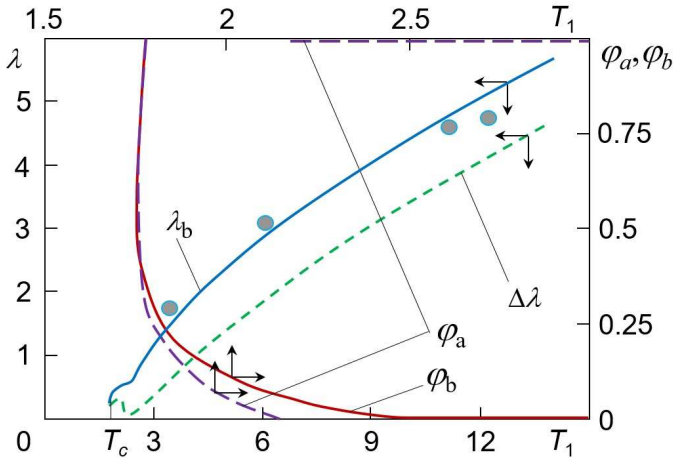

Figure 2. The parabolic growth rate constants λ, λ_b, the mushy layer width $\Delta\lambda = \lambda_b - \lambda_a$ and the volume fractions φ_a and φ_b as functions of the temperature difference T_1. The supercooling occurs at $T_1 > T_c \approx 1.776^{\circ}$C and $\lambda > 0.154$. The model parameters are [25]: $T_\infty = 15^{\circ}$C, $c_0 = 14$, $m = 0.4^{\circ}$C, $L = 3.35 \cdot 10^5$ J kg^{-1}, $D = 10^{-9}$ m^2 s^{-1}, $k_s = 2.219$ J m^{-1} s^{-1} $^{\circ}$C^{-1}, $k_l = 0.544$ J m^{-1} s^{-1} $^{\circ}$C^{-1}, $\rho_s = 920$ kg m^{-3}, $\rho_l = 1000$ kg m^{-3}, $C_{ps} = 2.01 \cdot 10^3$ J kg^{-1} $^{\circ}$C^{-1}, $C_{pl} = 4.187 \cdot 10^3$ J kg^{-1} $^{\circ}$C^{-1}. The circles show experimental data [27].

3. Unsteady-state crystallization scenario

Let us now consider a unidirectional process of binary system crystallization (e.g. sea water and ice) in the case of nonstationary boundary conditions at $z = 0$ (see Figure 1). Let the temperature at the cooled boundary $z = 0$ is an arbitrary function of time, i.e. $T = T_{at}(t)$ (e.g. atmospheric temperature in the case of sea water freezing).

3.1. Unsteady-state crystallization regime with a planar front

First we consider the thermally controlled heat transfer process, which is described by the temperature conductivity equation (1) in the solid phase (ice). If we treat the liquid phase (ocean) as isothermal, its temperature may be regarded as constant, i.e. $T = T_w$ at $z \geq h(t)$. Analyzing experimental data [23,28,29] and taking into account numerical solutions of the Stefan problem [30,31], we conclude that the temperature distribution in the solid phase, in some cases, is a nearly linear function of the spatial coordinate z. In this case, the temperature conductivity equation in the solid phase becomes $\partial^2 T/\partial z^2 = 0$. Physically it means that a relaxation time of the temperature field is many times smaller than a characteristic time of the phase interface motion. Thus, the temperature distribution obeys

$$T(z,t) = T_{at}(t) + \frac{T_w - T_{at}(t)}{h(t)} z, \ 0 \leq z \leq h(t). \tag{39}$$

The coordinate $h(t)$ of front motion is determined from the thermal balance condition, which takes the form

$$k_s \frac{\partial T}{\partial z} = \rho_s L \frac{dh}{dt}, \ z = h(t). \tag{40}$$

Combining equations (39) and (40), we get

$$h(t) = \sqrt{\frac{2k_s}{\rho_s L}\left(T_w t - \int_0^t T_{at}(\alpha)d\alpha\right)}, \tag{41}$$

where we consider the initial condition $h(0) = 0$.

The ice width and transient temperature profiles plotted accordingly to expressions (39) and (41) are demonstrated in Figure 3. It is easily seen that the frontal approximation differs from experiments. This discrepancy can be explained by the fact that, in real situations, the freezing process occurs in the presence of a phase transition (mushy) layer. The physical model of this process and its analytical solution are given in the next subsection.

3.2. Unsteady-state crystallization regime with a mushy layer

Let us now analyze the transient solidification scenario with a mushy layer shown in Figure 1. As before, we consider the linear temperature distribution in the solid phase, i.e.

$$T(z,t) = T_{at}(t) + C_1(t)z,\ 0 < z < a(t), \tag{42}$$

where C_1 represents an arbitrary function of time t.

The temperature distribution in the mushy layer will be regarded as linear too

$$T(z,t) = T_1(t) + T_2(t)z,\ a(t) < z < b(t), \tag{43}$$

where the time-dependent coefficients T_1 and T_2 are determined below. Note that the linear temperature profiles (42) and (43) follow from experimental data and numerical calculations [28–31].

We use here the Scheil equation [32, 33] to describe the mass transfer in a mushy region

$$\frac{\partial}{\partial t}\left[(1-\varphi)\,C\right] = 0,\ a(t) < z < b(t), \tag{44}$$

where C stands for the solute concentration (brine salinity) of a mushy layer.

The temperature and concentration fields in the phase transition layer are connected by means of the liquidus equation of the form

$$T = -mC,\ a(t) < z < b(t), \tag{45}$$

where m, as before, is the liquidus slope.

The boundary conditions imposed at the solid phase (ice) - mushy layer interface can be written as [25]

$$\varphi = \varphi_a,\ (T)_{z=a^-} = (T)_{z=a^+},\ z = a(t), \tag{46}$$

$$L_V\,(1-\varphi_a)\,\frac{da}{dt} = k_s\left(\frac{\partial T}{\partial z}\right)_{z=a^-} - \left[k_s\varphi_a + k_l\,(1-\varphi_a)\right]\left(\frac{\partial T}{\partial z}\right)_{z=a^+},\ z = a(t), \tag{47}$$

$$C_a\,(1-\varphi_a)\,\frac{da}{dt} = -D\,(1-\varphi_a)\left(\frac{\partial C}{\partial z}\right)_{z=a^+},\ z = a(t), \tag{48}$$

where $L_V = \rho_s L$ and subscript a designates the solid phase - mushy region interface.

At the mushy layer - liquid phase (ocean) interface, the boundary conditions take the form

$$\varphi = \varphi_b,\ (T)_{z=b^-} = (T)_{z=b^+} = T_w,\ z = b(t), \tag{49}$$

$$L_V\varphi_b\frac{db}{dt} = \left[k_s\varphi_b + k_l\,(1-\varphi_b)\right]\left(\frac{\partial T}{\partial z}\right)_{z=b^-},\ z = b(t), \tag{50}$$

where T_w is the constant temperature at $z \geq b(t)$ (constant sea water temperature) and subscript b denotes the mushy layer - liquid boundary.

Integration of equation (44) gives the solid fraction

$$\varphi(z,t) = 1 + \frac{(\varphi_b - 1)T_w}{T_1(t) + zT_2(t)}, \tag{51}$$

where expressions (43), (45) and (49) are taken into account.

Substituting now expressions (42), (43), (45) and (51) into the boundary conditions (46)-(50), we obtain

$$\varphi_a(t) = 1 + \frac{(\varphi_b - 1)T_w}{T_{at}(t) + C_1(t)a(t)}, \tag{52}$$

$$C_1(t) = \frac{(1-\varphi_a)L_V}{k_s}\frac{da}{dt} + \left[\varphi_a + K(1-\varphi_a)\right]T_2(t),\ K = \frac{k_l}{k_s}, \tag{53}$$

$$T_{at}(t) + C_1(t)a(t) = T_w + T_2(t)\left[a(t) - b(t)\right], \tag{54}$$

$$\left[T_2(t)\left(b(t) - a(t)\right) - T_w\right](1-\varphi_a)\frac{da}{dt} = D_w(1-\varphi_a)T_2(t), \tag{55}$$

$$T_2(t) = \frac{L_V\varphi_b}{\Phi}\frac{db}{dt},\ \Phi(\varphi_b) = k_s\varphi_b + k_l(1-\varphi_b), \tag{56}$$

$$T_1(t) = T_w - b(t)T_2(t). \tag{57}$$

The solid fraction at the boundary solid phase - mushy layer can be found from expressions (52), (54) and (56) as

$$\varphi_a(t) = 1 + \frac{(\varphi_b - 1)T_w}{T_w + (L_V\varphi_b/\Phi)(db/dt)\left[a(t) - b(t)\right]}. \tag{58}$$

Now combining expressions (55) and (56), we get

$$\left[\left(a(t) - b(t)\right)\frac{L_V\varphi_b}{\Phi}\frac{db}{dt} + T_w\right]\frac{da}{dt} = -\frac{DL_V\varphi_b}{\Phi}\frac{db}{dt}. \tag{59}$$

Substitution of functions $C_1(t)$ and $T_2(t)$ from equations (53) and (55) into condition (54) leads to the nonlinear differential equation of the form

$$L_V T_w(\varphi_b - 1)\left[(1-K)\frac{\varphi_b}{\Phi}\frac{db}{dt} - \frac{1}{k_s}\frac{da}{dt}\right]a(t)$$

$$= \left(T_w - T_{at}(t) - \frac{L_V\varphi_b}{\Phi}b(t)\frac{db}{dt}\right)\left[\left(a(t) - b(t)\right)\frac{L_V\varphi_b}{\Phi}\frac{db}{dt} + T_w\right]. \tag{60}$$

Here we used expression (58).

Equations (59) and (60) represent the nonlinear system for the determination of the moving boundaries $a(t)$ and $b(t)$. Below we consider three possible analytical solutions of these equations.

First of all, we consider the case when both boundaries evolve slowly [28, 29]. If this is really the case, neglecting the term proportional to $(da/dt)(db/dt)$ in equation (59), we come to

$$a(t) = -\frac{DL_V\varphi_b}{T_w\Phi}b(t), \tag{61}$$

where $a(0) = b(0) = 0$. Combining now equations (59) and (60) and substituting $a(t)$ from expression (61), we arrive at

$$b(t) = \sqrt{\frac{2}{I}\left(T_w t - \int_0^t T_{at}(\alpha)d\alpha\right)},\ I = \frac{L_V\varphi_b}{\Phi}\left[1 - \frac{DL_V\varphi_b}{T_w\Phi}\left(\frac{L_V D}{k_s T_w} + 1 - K\right)(\varphi_b - 1)\right]. \tag{62}$$

Secondly, if we consider the case of small temperature fluctuations, i.e.

$$|T_{at}(t)| \sim |T_w| \ll \frac{L_V \varphi_b}{\Phi} b(t) \frac{db}{dt},$$

we have from equations (59) and (60)

$$b(t) = Aa(t),\ a(t) = \sqrt{\frac{2D}{A-1}t},\ A = \sqrt{\frac{T_w(\varphi_b - 1)(1-K)\Phi}{DL_V\varphi_b}}. \tag{63}$$

Analytical solutions (63) describe the case when the phase transition interfaces $a(t)$ and $b(t)$ evolve as the square root of time and the solidification process is far from its initial stage [25, 34, 35].

Thirdly, let us consider the case when the solid phase - mushy layer boundary moves slower than the mushy layer - liquid phase boundary, i.e. when $da/dt \ll db/dt$. In this case, substitution of expression in square brackets from (59) into (60) gives

$$\frac{T_w}{2D}(\varphi_b - 1)(1-K)a^2(t) - \frac{L_V\varphi_b}{2\Phi}b^2(t) + T_w t - \int_0^t T_{at}(\alpha)d\alpha = 0.$$

Again, taking into consideration $a(t) \ll b(t)$, we finally obtain

$$a(t) = -D\int_0^t \frac{(T_w - T_{at}(\alpha))\,d\alpha}{T_{at}(\alpha)b(\alpha)},\ b(t) = \sqrt{\frac{2\Phi}{L_V\varphi_b}\left(T_w t - \int_0^t T_{at}(\alpha)d\alpha\right)}. \tag{64}$$

Thus, expressions (61)-(64) completely determine the evolution of phase transition boundaries $a(t)$ and $b(t)$ while the temperature distribution is governed by expressions (42), (43), (53), (56) and (57). The solute concentration and solid phase distributions therewith can be found from expressions (45) and (51).

The theory under consideration is compared with experimental data in Figure 3. The phase interfaces $a(t)$ and $b(t)$ are plotted in accordance with analytical solutions (61) and (62). All functions describing the mushy layer crystallization scenario essentially differ from the frontal solutions. Note that analytical solutions are in good agreement with experimental data.

4. Concluding remarks

Let us emphasize in conclusion that the unsteady-state interface dynamics determined by expressions (61), (62) and (64) becomes self-similar (i.e. becomes proportional to the square root of time) when the external (atmospheric) temperature T_{at} is constant. This conclusion connects the self-similar theory developed in Section 2 and the unsteady-state theory presented in Section 3. What is more, the phase transition boundaries $a(t)$ and $b(t)$ lie between their values corresponding to the maximum (T_{max}) and minimum (T_{min}) temperatures, that is

$$\sqrt{\frac{2}{I}(T_w - T_{max})\,t} \le b(t) \le \sqrt{\frac{2}{I}(T_w - T_{min})\,t}$$

in the case of interface dynamics (61) and (62).

The theory of interface dynamics in the presence of a phase transition (mushy) layer under consideration can be generalized to take into account the processes of nucleation and growth of particles in a metastable region. To do this, one can use the recently developed analytical theories of transient nucleation for single-component [36–38] and binary [39, 40] systems and analytical approaches under consideration.

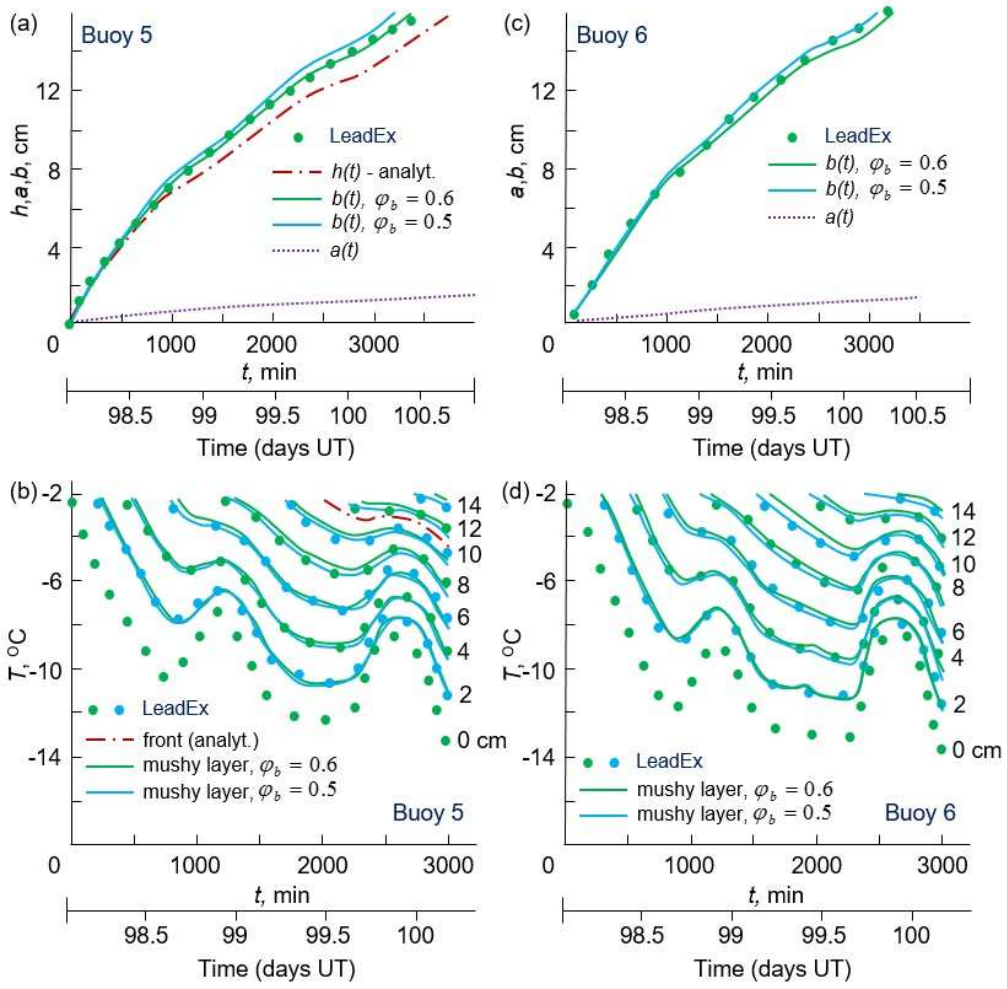

Figure 3. Ice thickness and temperature distributions as functions of time for (a), (b) buoy 5 and (c), (d) buoy 6 at lead 3 in accordance with the LeadEx experiment and the theory under consideration [28, 29]. The solid phase (ice) - liquid (ocean) interface is plotted by the dot-dashed line. Numbers at the curves corresponding to each line show the depths (in centimeters) measured from the ice/atmosphere interface $z = 0$. The temperature at $z = 0$ cm is the atmospheric temperature ($T_{at}(t)$). The time scale used by the LeadEx group is expressed in decimal days of 1992, abbreviated as UT and designated on the figure. The time origin in minutes corresponds to 0221, day 98 UT. Physical parameters used in calculations: $T_w = -2^{\mathrm{O}}\mathrm{C}$, $L_V = 3072{\cdot}10^5$ W·s·m^{-3}, $k_s = 2.03$ W·m^{-1}·$^{\mathrm{O}}$C^{-1}, $k_l = 0.56$ W·m^{-1}·$^{\mathrm{O}}$C^{-1}, $D = 1.2{\cdot}10^{-9}$ m^2·s^{-1}.

5. References

[1] Chalmers B 1961 *Physical Metallurgy* (New York: John Wiley)
[2] Flemings M 1974 *Solidification Processing* (New York: McGraw Hill)
[3] Kurz W and Fisher D J 1989 *Fundamentals of Solidification* (Aedermannsdorf: Trans. Tech. Publ.)
[4] Ivantsov G P 1951 *Dokl. Akad. Nauk SSSR* **81** 179–182
[5] Alexandrova I V, Alexandrov D V, Aseev D L and Bulitcheva S V 2009 *Acta Physica Polonica A* **115** 791–794
[6] Hoglund D E, Thompson M O and Aziz M J *Phys. Rev. B* **58** 189–199
[7] Mullins W W and Sekerka R F 1964 *J. Appl. Phys.* **35** 444–451
[8] Alexandrov D V and Ivanov A O 2000 *J. Crystal Growth* **210** 797–810
[9] Worster M G 1992 *J. Fluid Mech.* **237** 649–669

[10] Alexandrov D V 2004 *Int. J. Heat Mass Trans.* **47** 1383–1389
[11] Mansurov V 1990 *Mathl. Comput. Modelling* **14** 819–821
[12] Aseev D L and Alexandrov D V 2006 *Doklady Physics* **51** 291–295
[13] Alexandrov D V and Malygin A P 2012 *Int. J. Heat Mass Trans.* **55** 3196–3204
[14] Hills R N, Loper D E and Roberts P H 1983 *Q. J. Appl. Math.* **36** 505–539
[15] Fowler A C 1985 *IMA J. Appl. Math.* **35** 159–174
[16] Borisov V T 1987 *Theory of Two-Phase Zone of Metallic Ingot* (Moscow: Metallurgia)
[17] Alexandrov D V 2001 *J. Crystal Growth* **222** 816–821
[18] Alexandrov D V and Aseev D L 2005 *J. Fluid Mech.* **527** 57–66
[19] Aseev D L and Alexandrov D V 2006 *Acta Mater.* **54** 2401–2406
[20] Alexandrov D V and Malygin A P 2006 *Int. J. Heat Mass Trans.* **49** 763–769
[21] Alexandrov D V and Malygin A P 2006 *Dokl. Earth Sciences* **411** 1407–1411
[22] Alexandrov D V and Nizovtseva I G 2008 *Int. J. Heat Mass Trans.* **51** 5204–5208
[23] Alexandrov D V, Aseev D L, Nizovtseva I G, Huang H-N and Lee D 2007 *Int. J. Heat Mass Trans.* **50** 3616–3623
[24] Alexandrov D V, Nizovtseva I G, Malygin A P, Huang H-N and Lee D 2008 *J. Phys.: Condens. Matter* **20** 114105
[25] Worster M G 1986 *J. Fluid Mech.* **167** 481–501
[26] Batchelor G K 1974 *Ann. Rev. Fluid Mech.* **6** 227–255
[27] Huppert H E and Worsster M G 1985 *Nature* **314** 703–707
[28] Morison J, McPhee M, Muench R, Burke S, Coon M, D'Asaro E, Davidson K, Dillon T, Fairall C, Fernando J, Fett R, Francis J, Grenfell T, Jessup A, Lau P, Levine M, Onstott R, Overland J, Paulson C, Perovich D, Pinkel R, Richter-Menge J, Shuchman R, Smith D, Stanton T, Waggoner A, Weaver R and Wettlaufer J 1993 *Eos. Trans. AGU* **74** 393–397
[29] Wettlaufer J S, Worster M G and Huppert H E 2000 *J. Geophys. Res.* **105** 1123–1134
[30] Lee D and Alexandrov D V 2010 *Int. J. Pure Appl. Math.* **58** 381–416
[31] Lee D, Alexandrov D V and Huang H-N 2012 *Numer. Math. Theor. Meth. Appl.* **5** 157–185
[32] Scheil E 1942 *Z. Metall.* **34** 70–72.
[33] Kerr R C, Woods A W and Worster M G 1990 *J. Fluid Mech.* **216** 323–342
[34] Alexandrov D V and Ivanov A A 2009 *Int. J. Heat Mass Trans.* **52** 4807–4811
[35] Alexandrov D V, Ivanov A A and Malygin A P 2009 *Acta Physica Polonica A* **115** 795–799
[36] Alexandrov D V and Malygin A P 2013 *J. Phys. A: Math. Theor.* **46** 455101
[37] Alexandrov D V and Nizovtseva I G 2014 *Proc. R. Soc. A* **470** 20130647
[38] Alexandrov D V and Malygin A P 2014 *Modelling Simul. Mater. Sci. Eng.* **22** 015003
[39] Alexandrov D V 2014 *J. Phys. A: Math. Theor.* **47** 125102
[40] Alexandrov D V 2014 *Phil. Mag. Lett.* **94** 786–793

Acknowledgments

This work was supported by the Russian Science Foundation (grant no. 16-11-10095).